

Realization of strain induced multiple topological phases in Cu_2SnS_3 : An *ab-initio* study

Prakash Pandey^{1*} and Sudhir K. Pandey^{2†}

¹*School of Physical Sciences, Indian Institute of Technology Mandi, Kamand - 175075, India*

²*School of Mechanical and Materials Engineering, Indian Institute of Technology Mandi, Kamand - 175075, India*

(Dated: February 19, 2025)

The search of multiple topological phases (TPs) and their transitions by tuning different parameters through chemical substitutions, electric field, magnetic field, strain and Floquet engineering, etc has garnered a widespread attention in recent time. In spite of great effort, the observations of multiple TPs in a single material and multiple TP transitions in the presence of one parameter remain elusive. Here we demonstrate the presence of multiple TPs and their transitions with uniaxial compressive strain (UCS) in orthorhombic Cu_2SnS_3 by using *state-of-the-art ab-initio* calculations. In the absence of spin-orbit coupling (SOC), the Cu_2SnS_3 exhibits a single (type-II) nodal-ring and in the presence of SOC, it hosts Weyl phase with seven Weyl points (three at Γ and four at general positions) along with nodal arcs. On the application of UCS, it remains type-II nodal-ring < 5.5%, which further evolves into type-III nodal-ring for $5.5\% \leq \text{UCS} < 5.6\%$. Interestingly, at 5.6% of UCS, it shows Weyl phase with four Weyl nodes even in the absence of SOC. All the above-mentioned seven Weyl points persist below 5% of UCS. For $5\% \leq \text{UCS} < 5.6\%$, four Weyl points (at general positions) disappear and nodal-arcs remain intact in all the studied range of UCS. The TPs observed in the absence of SOC appears to arise due to the presence of strain driven topological flat band, which is typically reported to be seen in kagome and Lieb lattices.

Introduction.— The emergence of various exotic fermionic quasiparticles has fundamentally revolutionized the understanding of quantum states over the past few decades [1]. Dirac fermions in graphene [2–4], helical Dirac fermions at the surface of three-dimensional topological insulators [5–8], Majorana fermions in superconducting heterostructures [9–15], and the discovery of Weyl/Dirac semimetals [16–22] recently mark new frontiers in this field. These topological nontrivial states are driven by different fermionic quasiparticle excitations [23], including spin-1 fermions with threefold degeneracy carrying ± 2 topological charge, spin-3/2 Rarita-Schwinger-Weyl fermions with fourfold degeneracy carrying ± 4 topological charge [23–25], double Weyl fermions with ± 2 topological charge [26, 27], and double spin-1 fermions with sixfold degeneracy [28–30].

Usually, the energy spectrum of these quasiparticle excitations are described by $E_{\pm}(\mathbf{k}) = \sum_i k_i A_{i0} \pm \sqrt{\sum_j (\sum_i k_i A_{ij})^2} = T(\mathbf{k}) \pm U(\mathbf{k})$ [31]. Here, $T(\mathbf{k})$ and $U(\mathbf{k})$ are the kinetic and potential components of the energy spectrum. The most general Hamiltonian describing a Weyl point is $H(\mathbf{k}) = \sum_{ij} k_i A_{ij} \sigma_j$ [31], where k_i are components of the wave vector \mathbf{k} , σ_j are the Pauli matrices, and A_{ij} represents the coupling coefficients between the k_i and σ_j . The term $T(\mathbf{k})$, which is linear in momentum, decides the tilting of the cone-like spectrum. For example, if there exists a direction \mathbf{k} for which $T(\mathbf{k}) > U(\mathbf{k})$, then a type-II touching point appears [21, 31, 32]; otherwise, band touching is type-I.

Also, the linear dispersion along a specific \mathbf{k} direction is classified based on the behavior of the two touching bands: (i) opposite slopes correspond to type-I; (ii) identical slopes define type-II [31, 33, 34]; and (iii) one linear band with zero slope while that of the other one is nonzero is termed type-III nodal line [34–37].

A topological flat band (TFB) refers to dispersionless energy bands spanning the entire Brillouin zone, believed to be crucial for realizing fractional topological states without Landau levels [38–40]. Starting with Lieb’s work on the Hubbard model [41] and subsequently extended by Mielke [42] and Tasaki [43], research has expanded to include various lattice models based on line-graph construction [42, 44, 45], such as the kagome [38, 45], Lieb [41, 46], breathing-kagome [47–49], diatomic-kagome [50], coloring-triangle [51], and diamond-octagon lattices [52], as well as more recent studies on square and honeycomb lattices [53–56]. These advances have established material physics as a promising platform for realizing non-trivial physical phenomena such as excitonic insulator state [57], and the excited quantum anomalous/spin Hall effect [58].

Apart from this, however, only a few electronic TFB materials have been predicted, despite extensive theoretical and experimental studies [59–65]. Islam *et al.* [66] recently studied three-dimensional TFB in superlattices of the HgTe class of materials. In their work, they reported a nodal-line semimetal characterized by two isoenergetic, circular nodal-rings at the Fermi level. Furthermore, under compressive hydrostatic pressure, they found that the superlattice exhibits a trivial insulating state, whereas the unstrained superlattice behaves as an ideal Weyl semimetal. However, in this class of superlattice materials, topological phases evolve in the presence

* prakashpandey6215@gmail.com

† sudhir@iitmandi.ac.in

of hydrostatic pressure. Naturally, two unresolved questions arise: First, can the coexistence of a TFB and nodal line near the Fermi level be realized without requiring superlattice? Second, can these features be tailored by applying external strain? To our knowledge, the coexisting features has not been explored in orthorhombic body-centered lattices. However, multiple topological phases and their transitions have been observed to arise by tuning different parameters through chemical substitutions, electric fields, magnetic fields, strain, and Floquet engineering, etc [67–71]. In the present work, we systematically investigate the coexistence of TFB with nodal line semimetals in Cu_2SnS_3 using first-principles calculations. Furthermore, we have also investigated the evolution of topological phases as a function of uniaxial strain. The presence of nodal-line phases in unstrained Cu_2SnS_3 and the strain engineering that produces emergent phases, such as TFB, in this material prove its importance, as such features are rarely found. Studying the topological transport properties arising from the presence of TFB in this material will be an interesting avenue for future research. Apart from this, the Weyl phase of Cu_2SnS_3 as a function of uniaxial strain in the presence of SOC is also investigated. Our findings reveal the coexistence of seven Weyl points (three at Γ and four at general positions) as well as nodal arcs, which have been lacking in earlier studies and are highly important for deepening our fundamental understanding of topological states of matter. Revealing such topological phases in this material offers a new platform to study similar systems that host these features.

Computational details.— Using the first-principles approach, we have used the WIEN2k package [72] to calculate the ground state energy of orthorhombic Cu_2SnS_3 . The generalized gradient approximation (GGA) [73] within the Perdew-Burke-Ernzerhof is preferred as an exchange-correlation (XC) functional. This XC functional is used to optimize the geometry and lattice constant. The optimized lattice parameters are $a=11.61$ Å, $b=3.92$ Å, and $c=5.43$ Å. The relaxed wyckoff positions of Cu, Sn, S1, and S2 are (0.8297, 0.5, 0.49053), (0.0, 0.0, 0.018978), (0.82306, 0.0, 0.26436), and (0.5, 0.0, 0.22018), respectively. A $12\times 12\times 12$ k -mesh size is used for the self-consistent calculations. Furthermore, the energy convergence limit for the self-consistent method is set to 10^{-7} Ry/cell for the calculations. The analysis of Weyl nodes and nodal lines was performed using our in-house code, PY-Nodes [74], which is based on the Nelder-Mead function minimization method [75, 76]. To calculate the topological charge or chirality for each Weyl point, we have used the WLoopPHI code [77]. To investigate topological properties such as surface states and Fermi arcs, a tight-binding (TB) model based on maximally localized Wannier functions (MLWF) is obtained using the WANNIER90 code [78]. The surface state calculations are performed using the WANNIERTOOLS package [79].

Material realization.— Recently, the symmorphic $Imm2$ -phase of the Cu_2SnS_3 class of materials has

been theoretically reported as a new type of topological semimetal. In particular, Cu_2SnS_3 exhibits a diverse range of phases, including monoclinic, cubic, tetragonal, hexagonal, and orthorhombic, associated with the Cc , $F\bar{4}3m$, $I\bar{4}2m$, $P6_3/mmc$, and $Imm2$ space group symmetries, respectively [80–84]. The Cc and $F\bar{4}3m$ phases of this compound have been synthesized and systematically studied for their electronic and vibrational properties through experiments and *first-principles* calculations. The electronic and phononic topological transport properties of the $Imm2$ phase of this material remain unexplored from both experimental and theoretical perspectives. Therefore, it is necessary to first study their electronic topological properties in the absence and presence of strain.

In the absence of SOC.— The electronic band structure of Cu_2SnS_3 in Fig. 1 (a) displays important features. First, we find that the band touching (2-3) appears along X- Γ high-symmetry path with a linear dispersion at the energy ~ 105 meV, which is above the Fermi level. However, a zoomed-in scale of the figure shows a gap of ~ 5.6 meV between bands 2 and 3. This indicates that along X- Γ high-symmetry path, topological quantum phases are absent. Therefore, it is necessary to search for band-touching points in the entire Brillouin zone (BZ). Consequently, we have searched for band-touching points in the entire BZ and found that they form a nodal line. The obtained nodal line lies in the k_x - k_z plane with $k_y=0$, as shown in the subplot of Fig. 1 (a). Since the $Imm2$ phase of this material possesses two mirror reflection symmetries, M_x and M_y as well as a twofold rotation little group symmetry C_{2z} , a detailed analysis of the symmetry operations reveals that along the X- Γ high symmetric line, the touching bands have opposite mirror eigenvalues for M_x [84]. This indicates that the touching point is protected by the mirror reflection symmetry M_x [84]. To determine the nature of the obtained nodal line, we calculated the energy spectrum around the obtained node points. The corresponding results are shown in Fig. 1 (b). The 3D representation of the energy spectrum with respect to the wave vector \mathbf{k} reveals that both bands have identical slopes. Such band-dispersion is commonly referred to as type-II [32]. This indicates that the low-energy excitations in Cu_2SnS_3 may correspond to type-II nodal-line fermions in the absence of SOC [21, 31]. To verify whether the touching points in the 3D representation of the energy spectrum indeed form a nodal ring, we calculated the 2D projection where the two bands are degenerate at the \mathbf{k} -points (see Fig. 1 and corresponding text in the SM [85]). The figure clearly indicates that the bands form a nodal ring in the k_x - k_z plane with $k_y = 0$. Therefore, we conclude that Cu_2SnS_3 is a type-II nodal-line semimetal.

Strain has proven to be a powerful and effective approach for engineering the electronic properties of quantum materials by tuning their band structures. Here, we investigate the impacts of strain on the dispersion curves, which directly influence the topological proper-

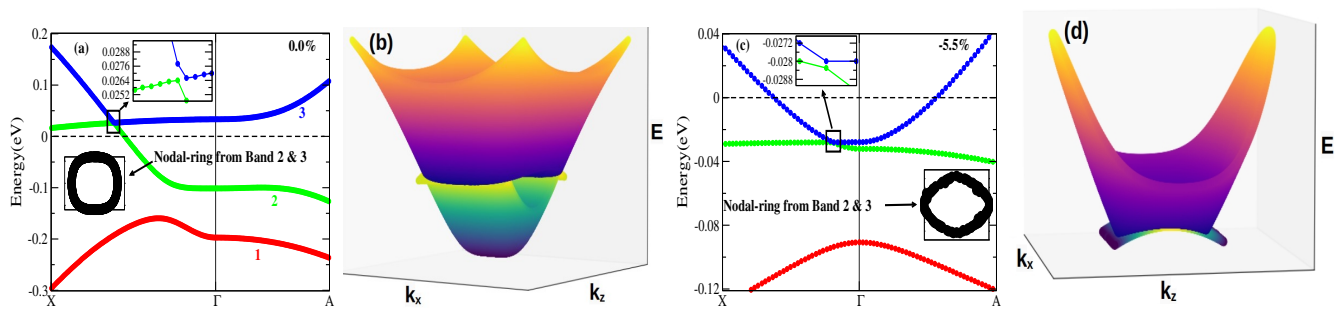


FIG. 1: (Color online) Evolution of bulk band structure of Cu_2SnS_3 along high-symmetry points X- Γ -A in the first BZ under uniaxial strains in different magnitudes when SOC is excluded. The negative sign in the figures stands uniaxial compressive strain (UCS) along the a axis. The red, green and blue curves represent the band number 1, 2 and 3, respectively. Zero energy represents the Fermi level. (a) and (c) plots show the energy dispersions at 0% and 5.5% UCS, respectively. The subplot of (a) and (c) show the energy-gap between band 2 and 3 along X- Γ direction. We show the obtained topological nodal line in (a) and (c) at different magnitudes of strain in the first BZ apart from the X- Γ -A direction. (b)((d)) 3D representation of the energy (E) dispersions at 0 (-5.5)% strain around type-II (type-III) nodal-line in the k_x - k_z plane.

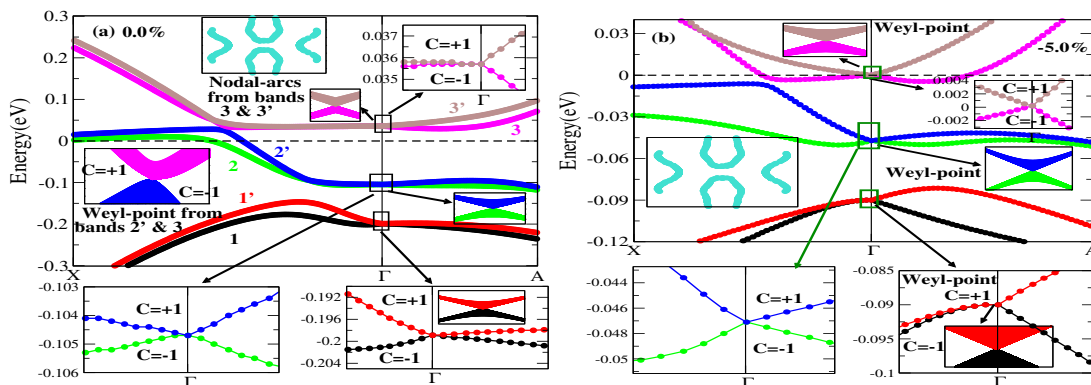


FIG. 2: (Color online) Evolution of bulk band structure of Cu_2SnS_3 along high-symmetry direction X- Γ -A in the first BZ under uniaxial strains in different magnitudes when SOC is included. The negative sign in the figures stands UCS along the a axis. The black, red, green blue, magenta and brown curves represent the band number 1, 1', 2, 2', 3 and 3', respectively. (a) and (b) plots show the energy dispersions at 0% and 5.5% UCS. We show the zoom-up of the touching of different combinations of bands. The chiralities (C) for each band are also indicated in the plots. The coordinates of the Weyl point between bands 2' and 3 are $(\pm \frac{2\pi}{a}(0.226), \pm \frac{2\pi}{b}(0.004), 0.000)$, and the energy dispersion around the obtained Weyl point is shown in subplot (a). We also show the nodal arc in the subplot of Fig. (a) and (b).

ties of quantum materials. Considering the directionally dependent properties, we applied uniaxial compressive strains (UCS) along the a axis, ranging from 0% to 6%, which are achievable in experiments. We have calculated the electronic dispersion for each strained structure of Cu_2SnS_3 in the absence of SOC and observed how the dispersion evolves with different magnitudes of strain. It is found that at 5% compressive strain, the band-touching points come very close to the Fermi level (see Fig. 2 and corresponding text in the SM [85]). At this strain value (5%), one of the linear band becomes nearly flat, indicating a transition from type-II to quasi type-III dispersion. This type of dispersion leads to a quasi-type-III nodal line. A quasi-type-III nodal line suggests a hybrid nature, where features of both types II and III coexist. In addition to this, the area covered by the nodal line decreases as the compressive strain value increases (see details in the SM [85]). With the further application of a 5.5% com-

pressive strain, the situation becomes markedly different from the unstrained structure. At this point, quasi-type-III dispersion transitions into type-III, which results in the formation of type-III nodal line. The corresponding band structure and 3D representation of the energy spectrum are shown in Figs. 1 (c)-(d). From Fig. 1 (d), it is seen that one of the energy bands is dispersionless across the entire $k_y=0$ plane. This type of energy band-dispersion is generally referred to as type-III. Moreover, we have also plotted the projection of the two touching 3D dispersion bands onto k_x - k_z plane, where the intersection forms a nodal line (see Fig. 3 and corresponding text in the SM [85]). From the above discussion, it is revealed that at 5.5% strain, Cu_2SnS_3 exhibits a type-III nodal line. Furthermore, with the application of a 5.6% compressive strain, the type-III nodal line transforms into Weyl points (see Fig. 4 and corresponding text in the SM [85]). This is another interesting result

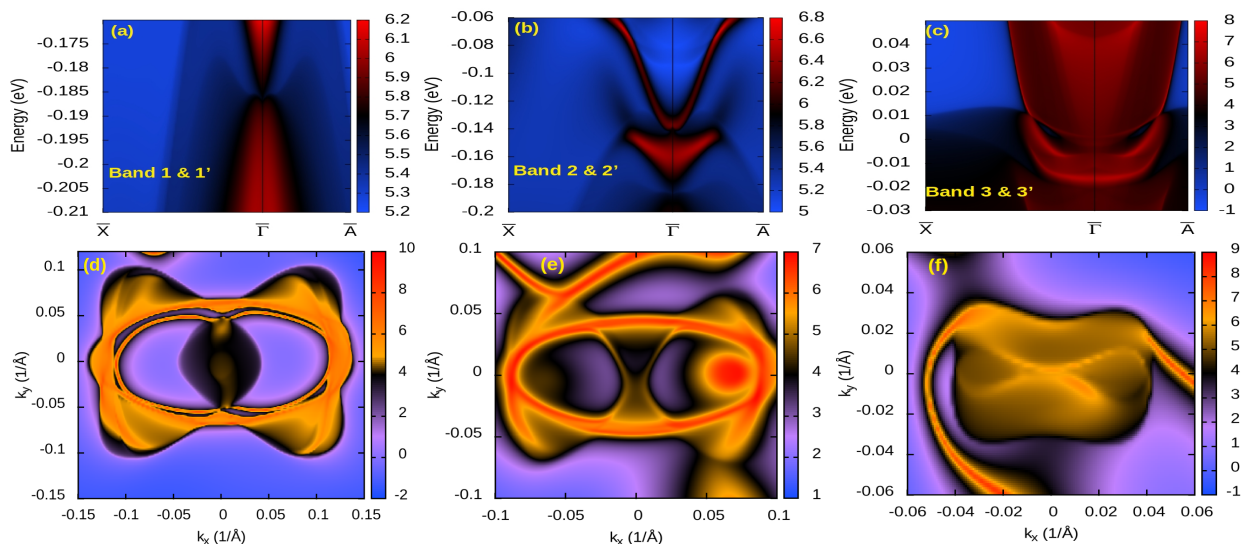


FIG. 3: (Color online) Surface density of states for the (001) surface (a) band 1-1', (b) band 2-2', and (c) band 3-3' of Cu_2SnS_3 at 0% strain along two dimensional high-symmetric directions. (d)-(f) plot show non-trivial topological Fermi arcs of Cu_2SnS_3 of (001) surface for band 1-1' at energy -185 meV, band 2-2' at energy -104.5 meV and band 3-3' at energy 35.5 meV for the top surface of the unit cell.

that the band topology changes after 5.5% compressive strain, leading to the appearance of Weyl nodes. To confirm whether it is indeed a Weyl node at this strain value, we have calculated the chirality and found it to be ± 1 . Thus, the obtained results reveal the presence of several topological phases under compressive strain ranging from 0% to 5.6%, including a type-II nodal line at 0%, a quasi-type-III nodal line phase at 5%, a type-III nodal line phase at 5.5%, and a Weyl point at 5.6%. Therefore, the application of external strain enables the realization of multiple topological phases, offering a promising platform for exploring non-trivial physical phenomena. In experiments, these topological phase transitions can be achieved by applying appropriate uniaxial compressive stress.

The above discussion reveals that electronic dispersions are highly sensitive to mechanical strain. At this point, we focus on another interesting feature: the topological three-dimensional flat band, which is highly non-trivial because it is typically reported in special types of lattices such as kagome and Lieb or twisted bilayer/trilayer graphene [86–90]. However, when applying a 5.6% UCS on Cu_2SnS_3 , we reveal a topological flat band in the system, which is reported in an orthorhombic body-centered lattice. Moreover, hydrostatic pressure and uniaxial strain are powerful methods to achieve topological flat bands. For example, earlier studies [66] on superlattices of the HgTe class of materials (with space group $F43m$) demonstrated how topological phases evolve as a function of hydrostatic pressure and uniaxial strain. Therefore, the emergence of a topological flat band through uniaxial strain is highly significant, as this approach allows achieving the feature simply by applying strain, without the need to create superlattices or

introduce disorder into the system.

In the presence of SOC.— Spin-orbit coupling (SOC) interactions are a key ingredient for generating non-trivial topological properties. In Cu_2SnS_3 , the effect of SOC plays a vital role in exhibiting topologically non-trivial properties. SOC splits band 2 (3) into 2 and 2' (3 and 3') along the X- Γ -A high-symmetry path, as shown in Fig. 2 (a). However, the degeneracy is preserved between bands 2' and 3. This accidental degeneracy leads to a Weyl point with chirality (C) ± 1 . The co-ordinates of the obtained Weyl point are $(\pm \frac{2\pi}{a}(0.226), \pm \frac{2\pi}{b}(0.004), 0.000)$. Furthermore, band 1 splits into 1 and 1', resulting in a Weyl point near -198 meV at the Γ point. Similarly, band 2 (3) splits into bands 2-2' (3-3'), which also produces Weyl points near -104.5 (35.5) meV, at the Γ point. Notably, another interesting feature is observed: the presence of a nodal-arcs between bands 3 and 3', as shown in the inset of Fig. 2 (a). Therefore, in the unstrained structure with SOC included, the coexistence of both Weyl nodes and nodal-lines distinguishes this material from others. Interestingly, such a coexistence has not been reported in previous studies [84]. The possible reason for this may be the use of MLWFs, which are employed to construct the TB model for predicting the topological quantum phases of the material. To obtain an accurate TB Hamiltonian, good Wannier fitting is essential because the bands and projectors play a significant role in achieving a reliable TB Hamiltonian. It is also important to keep in mind that highly accurate results may not be expected from an empirical tight-binding model [91]. Therefore, there is a high chance of missing important topological quantum phases present in the material. From Fig. 2 (b), an interesting and important result is observed: upon applying 5% UCS, the degen-

eracy of bands 2' and 3 is lifted, creating a gap of 5.86 meV. However, for UCS up to <5%, the Weyl phase remains robust, but the coordinates of the Weyl point shift from $(\pm \frac{2\pi}{a}(0.226), \pm \frac{2\pi}{b}(0.004), 0.000)$ to $(\pm \frac{2\pi}{a}(0.099), \pm \frac{2\pi}{b}(0.003), 0.000)$. This indicates that the presence of Weyl points in the unstrained structure is due to accidental degeneracy between bands 2' and 3, which is lifted upon applying UCS $\geq 5\%$. Similar studies are done with varying magnitudes of UCS, and we found similar results for each strain value (see Fig. 5 and corresponding text in the SM [85]). Also, for each values of strain up to <5%, we found only four Weyl points, indicating the minimal number of Weyl points that a system with time-reversal invariance can host (see details of coordinates of the Weyl points as mentioned in Table 1 of the SM [85]).

To determine whether these degeneracies lead to topologically nontrivial states, we have further calculated the surface states and Fermi arcs along X- Γ -A high-symmetric direction. The corresponding results are shown in Figs. 3 (a)-(f). To calculate the surface states, one first obtains the tight-binding parameters for the bulk and surface atoms in order to study the non-trivial topological properties. The high-symmetry points (X, Γ and A) of the 3D momentum space are projected onto the (001) surface. Therefore, the X, Γ and A points are now denoted by \bar{X} , $\bar{\Gamma}$ and \bar{A} , respectively. This direction was chosen because linear touching is observed at the Γ point. From the figures, it is evident that linear touchings occur between bands 1-1', 2-2', and 3-3' at energies of -185 meV, -104.5 meV, and 35.5 meV, respectively. For the experimental detection of the topological character of the Weyl point, it is essential to analyze the surface spectrum that hosts Fermi arcs, as the presence of non-trivial Fermi arcs is a hallmark of Weyl semimetals. Thus, we have calculated the Fermi arc, as shown in Figs. 3 (d)-(f), for bands 1-1' at an energy of -185 meV, bands 2-2' at -104.5 meV, and bands 3-3' at 35.5 meV. Since there is only one Weyl point located at Γ , it is expected that the Fermi arc originates and merges at the Γ point, forming a closed loop. The results obtained in Fig. 3 (d) are in accordance with this discussion. From the figure, it can be seen that the non-trivial Fermi arc forms

a closed loop. The shape of the Fermi arcs for different combinations of bands changes as we move from band 1 to band 3'. However, the features of the Fermi arcs for bands 2-2' and 3-3' are the same as those of the Fermi arc for band 1-1'. The existence of such Fermi arcs signifies a non-trivial topological phase in the system, and their presence is intrinsically linked to systems with a non-zero Chern number. A similar behavior is observed in this material at each compressive strain value (-5%, -5.5%, and -5.6%). In addition, we have also discussed the topological surface states and Fermi arcs, which enclose 4 Weyl points $(\pm \frac{2\pi}{a}(0.226), \pm \frac{2\pi}{b}(0.004), 0.000)$ (see Fig. 6 in the SM [85]). Therefore, based on the above results, it is concluded that a Weyl point exists at the Γ point. This theoretical prediction can potentially be verified through corresponding experimental studies. Furthermore, the predicted result highlights the potential of Cu_2SnS_3 for various practical applications.

Conclusions and Outlook.— In summary, using *ab-initio* calculations, we have investigated the evolution of multiple topological phases and their transitions as a function of uniaxial strain in orthorhombic Cu_2SnS_3 . In the absence of SOC, the material shows a type-II nodal-ring and in the presence of SOC, it exhibit Weyl phase with seven Weyl points (three at Γ and four at $(\pm \frac{2\pi}{a}(0.226), \pm \frac{2\pi}{b}(0.004), 0.000)$ positions) along with nodal arcs. Notably, type-II nodal-ring persists up to a UCS of < 5.5%. However, at 5.5 (5.6)% UCS, a type-III nodal-ring (Weyl point) emerges. The type-III nodal-line phase realized in the present work is useful for searching materials with carriers residing in flat energy bands, leading to various emerging phenomena such as strong nonlinear optical responses and large magnetoresistance or magneto-elastoresistance. In the presence of SOC, for $5\% \leq \text{UCS} < 5.6\%$, four Weyl points at $(\pm \frac{2\pi}{a}(0.226), \pm \frac{2\pi}{b}(0.004), 0.000)$ positions vanish, while nodal arcs remain intact throughout the studied range of UCS. The presence of multiple topological phases in Cu_2SnS_3 and multiple topological phase transitions under uniaxial strain highlight its importance, making it an interesting material for future research.

-
- [1] P. B. Pal, *American Journal of Physics* **79**, 485 (2011).
 - [2] A. H. Castro Neto, F. Guinea, N. M. R. Peres, K. S. Novoselov, and A. K. Geim, *Rev. Mod. Phys.* **81**, 109 (2009).
 - [3] K. S. Novoselov, A. K. Geim, S. V. Morozov, D. Jiang, M. I. Katsnelson, I. V. Grigorieva, S. V. Dubonos, and A. A. Firsov, *nature* **438**, 197 (2005).
 - [4] C.-H. Park, L. Yang, Y.-W. Son, M. L. Cohen, and S. G. Louie, *Nature Physics* **4**, 213 (2008).
 - [5] M. Z. Hasan and C. L. Kane, *Rev. Mod. Phys.* **82**, 3045 (2010).
 - [6] Y. Ando, *Journal of the Physical Society of Japan* **82**, 102001 (2013).
 - [7] X. Zhou, C. Fang, W.-F. Tsai, and J. Hu, *Phys. Rev. B* **80**, 245317 (2009).
 - [8] H. Beidenkopf, P. Roushan, J. Seo, L. Gorman, I. Drozdov, Y. S. Hor, R. J. Cava, and A. Yazdani, *Nature Physics* **7**, 939 (2011).
 - [9] V. Mourik, K. Zuo, S. M. Frolov, S. R. Plissard, E. P. A. M. Bakkers, and L. P. Kouwenhoven, *Science* **336**, 1003 (2012).
 - [10] S. Nadj-Perge, I. K. Drozdov, J. Li, H. Chen, S. Jeon, J. Seo, A. H. MacDonald, B. A. Bernevig, and A. Yazdani, *Science* **346**, 602 (2014).
 - [11] M. Sato and Y. Ando, *Reports on Progress in Physics* **80**, 076501 (2017).

- [12] A. Das, Y. Ronen, Y. Most, Y. Oreg, M. Heiblum, and H. Shtrikman, *Nature Physics* **8**, 887 (2012).
- [13] R. M. Lutchyn, J. D. Sau, and S. Das Sarma, *Phys. Rev. Lett.* **105**, 077001 (2010).
- [14] G. Sharma and S. Tewari, *Phys. Rev. B* **93**, 195161 (2016).
- [15] C. Beenakker, *Annu. Rev. Condens. Matter Phys.* **4**, 113 (2013).
- [16] N. P. Armitage, E. J. Mele, and A. Vishwanath, *Rev. Mod. Phys.* **90**, 015001 (2018).
- [17] M. Phillips and V. Aji, *Phys. Rev. B* **90**, 115111 (2014).
- [18] A. A. Burkov, M. D. Hook, and L. Balents, *Phys. Rev. B* **84**, 235126 (2011).
- [19] A. Ahmad, G. V. K, and G. Sharma, *Journal of Physics: Condensed Matter* **37**, 043001 (2024).
- [20] C. Fang, Y. Chen, H.-Y. Kee, and L. Fu, *Phys. Rev. B* **92**, 081201 (2015).
- [21] S.-Y. Xu, N. Alidoust, G. Chang, H. Lu, B. Singh, I. Belopolski, D. S. Sanchez, X. Zhang, G. Bian, H. Zheng, M.-A. Hsuan, Y. Bian, S.-M. Huang, C.-H. Hsu, T.-R. Chang, H.-T. Jeng, A. Bansil, T. Neupert, V. N. Strocov, H. Lin, S. Jia, and M. Z. Hasan, *Science Advances* **3**, e1603266 (2017).
- [22] N. B. Kopnin, T. T. Heikkilä, and G. E. Volovik, *Phys. Rev. B* **83**, 220503 (2011).
- [23] P. Tang, Q. Zhou, and S.-C. Zhang, *Phys. Rev. Lett.* **119**, 206402 (2017).
- [24] L. Liang and Y. Yu, *Phys. Rev. B* **93**, 045113 (2016).
- [25] M. Ezawa, *Phys. Rev. B* **94**, 195205 (2016).
- [26] C. Fang, M. J. Gilbert, X. Dai, and B. A. Bernevig, *Phys. Rev. Lett.* **108**, 266802 (2012).
- [27] Y. Xu and L.-M. Duan, *Phys. Rev. A* **94**, 053619 (2016).
- [28] B. Bradlyn, J. Cano, Z. Wang, M. G. Vergniory, C. Felser, R. J. Cava, and B. A. Bernevig, *Science* **353**, aaf5037 (2016).
- [29] G. Chang, S.-Y. Xu, B. J. Wieder, D. S. Sanchez, S.-M. Huang, I. Belopolski, T.-R. Chang, S. Zhang, A. Bansil, H. Lin, and M. Z. Hasan, *Phys. Rev. Lett.* **119**, 206401 (2017).
- [30] S. Nie, B. A. Bernevig, and Z. Wang, *Phys. Rev. Res.* **3**, L012028 (2021).
- [31] A. A. Soluyanov, D. Gresch, Z. Wang, Q. Wu, M. Troyer, X. Dai, and B. A. Bernevig, *Nature* **527**, 495 (2015).
- [32] J. He, X. Kong, W. Wang, and S.-P. Kou, *New Journal of Physics* **20**, 053019 (2018).
- [33] S. Li, Z.-M. Yu, Y. Liu, S. Guan, S.-S. Wang, X. Zhang, Y. Yao, and S. A. Yang, *Phys. Rev. B* **96**, 081106 (2017).
- [34] Q.-B. Liu, Z.-D. Guo, F.-F. Du, D.-M. Feng, X.-Y. Tan, Z. Yu, and L. Xiong, *Journal of Physics: Condensed Matter* **36**, 325703 (2024).
- [35] X.-P. Li, K. Deng, B. Fu, Y. Li, D.-S. Ma, J. Han, J. Zhou, S. Zhou, and Y. Yao, *Phys. Rev. B* **103**, L081402 (2021).
- [36] B. Zheng, B. Xia, R. Wang, Z. Chen, J. Zhao, Y. Zhao, and H. Xu, *Phys. Rev. B* **101**, 100303 (2020).
- [37] Z. Lv, N. Jia, J. Cai, X. Jiang, J. Zhao, and Z. Liu, *Phys. Rev. B* **106**, 195429 (2022).
- [38] E. Tang, J.-W. Mei, and X.-G. Wen, *Phys. Rev. Lett.* **106**, 236802 (2011).
- [39] K. Sun, Z. Gu, H. Katsura, and S. Das Sarma, *Phys. Rev. Lett.* **106**, 236803 (2011).
- [40] Y.-F. Wang, Z.-C. Gu, C.-D. Gong, and D. N. Sheng, *Phys. Rev. Lett.* **107**, 146803 (2011).
- [41] E. H. Lieb, *Phys. Rev. Lett.* **62**, 1201 (1989).
- [42] A. Mielke, *Journal of Physics A: Mathematical and General* **24**, L73 (1991).
- [43] H. Tasaki, *Phys. Rev. Lett.* **69**, 1608 (1992).
- [44] A. Mielke, *Journal of Physics A: Mathematical and General* **24**, 3311 (1991).
- [45] A. Mielke, *Journal of Physics A: Mathematical and General* **25**, 4335 (1992).
- [46] H. Tasaki, *Progress of Theoretical Physics* **99**, 489 (1998).
- [47] M. Ezawa, *Phys. Rev. Lett.* **120**, 026801 (2018).
- [48] A. Bolens and N. Nagaosa, *Phys. Rev. B* **99**, 165141 (2019).
- [49] H. Xue, Y. Yang, F. Gao, Y. Chong, and B. Zhang, *Nature materials* **18**, 108 (2019).
- [50] Y. Zhou, G. Sethi, C. Zhang, X. Ni, and F. Liu, *Phys. Rev. B* **102**, 125115 (2020).
- [51] S. Zhang, M. Kang, H. Huang, W. Jiang, X. Ni, L. Kang, S. Zhang, H. Xu, Z. Liu, and F. Liu, *Phys. Rev. B* **99**, 100404 (2019).
- [52] B. Pal, *Phys. Rev. B* **98**, 245116 (2018).
- [53] H. Liu, G. Sethi, S. Meng, and F. Liu, *Phys. Rev. B* **105**, 085128 (2022).
- [54] C. Wu, D. Bergman, L. Balents, and S. Das Sarma, *Phys. Rev. Lett.* **99**, 070401 (2007).
- [55] C. Wu and S. Das Sarma, *Phys. Rev. B* **77**, 235107 (2008).
- [56] M. Zhou, Z. Liu, W. Ming, Z. Wang, and F. Liu, *Phys. Rev. Lett.* **113**, 236802 (2014).
- [57] G. Sethi, Y. Zhou, L. Zhu, L. Yang, and F. Liu, *Phys. Rev. Lett.* **126**, 196403 (2021).
- [58] Y. Zhou, G. Sethi, H. Liu, Z. Wang, and F. Liu, *Nanotechnology* **33**, 415001 (2022).
- [59] M. G. Yamada, T. Soejima, N. Tsuji, D. Hirai, M. Dincă, and H. Aoki, *Phys. Rev. B* **94**, 081102 (2016).
- [60] X. Zhang, Z. Wang, M. Zhao, and F. Liu, *Phys. Rev. B* **93**, 165401 (2016).
- [61] H. Tanaka, Y. Fujisawa, K. Kuroda, R. Noguchi, S. Sakuragi, C. Bareille, B. Smith, C. Cacho, S. W. Jung, T. Muro, Y. Okada, and T. Kondo, *Phys. Rev. B* **101**, 161114 (2020).
- [62] O. J. Silveira and H. Chacham, *Journal of Physics: Condensed Matter* **29**, 09LT01 (2017).
- [63] Y. Gao, Y.-Y. Zhang, J.-T. Sun, L. Zhang, S. Zhang, and S. Du, *Nano Research* **13**, 1571 (2020).
- [64] L. Zhang, Z. Wang, B. Huang, B. Cui, Z. Wang, S. Du, H.-J. Gao, and F. Liu, *Nano Letters* **16**, 2072 (2016).
- [65] Z. Wang, N. Su, and F. Liu, *Nano letters* **13**, 2842 (2013).
- [66] R. Islam, B. Ghosh, G. Cuono, A. Lau, W. Brzezicki, A. Bansil, A. Agarwal, B. Singh, T. Dietl, and C. Autieri, *Phys. Rev. Res.* **4**, 023114 (2022).
- [67] H. Yuan, M. S. Bahramy, K. Morimoto, S. Wu, K. Nomura, B.-J. Yang, H. Shimotani, R. Suzuki, M. Toh, C. Kloc, *et al.*, *Nature Physics* **9**, 563 (2013).
- [68] H. Nakamura and T. Kimura, *Phys. Rev. B* **80**, 121308 (2009).
- [69] T. Tantt, B. Hensen, K. W. Chan, C. H. Yang, W. W. Huang, M. Fogarty, F. Hudson, K. Itoh, D. Culcer, A. Laucht, A. Morello, and A. Dzurak, *Phys. Rev. X* **9**, 021028 (2019).
- [70] K. Zollner, S. a. M. João, B. K. Nikolić, and J. Fabian, *Phys. Rev. B* **108**, 235166 (2023).
- [71] K. W. Lee, M. J. A. Calderon, X.-L. Yu, C. H. Lee, Y. S. Ang, and P.-H. Fu, *Phys. Rev. B* **111**, 045406 (2025).
- [72] P. Blaha, K. Schwarz, F. Tran, R. Laskowski, G. K. Madsen, and L. D. Marks, *J. Chem. Phys.* **152**, 074101 (2020).

- [73] J. P. Perdew, K. Burke, and M. Ernzerhof, *Phys. Rev. Lett.* **77**, 3865 (1996).
- [74] V. Pandey and S. K. Pandey, *Comput. Phys. Comm.* **283**, 108570 (2023).
- [75] J. A. Nelder and R. Mead, *The Computer Journal* **7**, 308 (1965).
- [76] P. Pandey and S. K. Pandey, *Computer Physics Communications* **303**, 109281 (2024).
- [77] H. Saini, M. Laurien, P. Blaha, and O. Rubel, *Computer Physics Communications* **270**, 108147 (2022).
- [78] A. A. Mostofi, J. R. Yates, Y.-S. Lee, I. Souza, D. Vanderbilt, and N. Marzari, *Computer physics communications* **178**, 685 (2008).
- [79] Q. Wu, S. Zhang, H.-F. Song, M. Troyer, and A. A. Soluyanov, *Comput. Phys. Comm.* **224**, 405 (2018).
- [80] M. Onoda, X. an Chen, A. Sato, and H. Wada, *Materials Research Bulletin* **35**, 1563 (2000).
- [81] X. an Chen, H. Wada, A. Sato, and M. Mieno, *Journal of Solid State Chemistry* **139**, 144 (1998).
- [82] C. Wu, Z. Hu, C. Wang, H. Sheng, J. Yang, and Y. Xie, *Applied Physics Letters* **91**, 143104 (2007).
- [83] P. A. Fernandes, P. M. P. Salomé, and A. F. da Cunha, *physica status solidi c* **7**, 901 (2010).
- [84] L. Zhou, Y. Qian, C. Yue, Y. Jiang, Z. Fang, W. Zhang, C. Fang, and H. Weng, *Phys. Rev. Res.* **4**, 033067 (2022).
- [85] P. Pandey and S. K. Pandey, See Supplemental Material.
- [86] H. J. Kim, M. J. Kim, J. Lee, J. M. Ok, and C.-J. Kang, *Phys. Rev. B* **110**, 024504 (2024).
- [87] H. Yuan, W. Zhang, Q. Pei, and X. Zhang, *Phys. Rev. B* **109**, L041109 (2024).
- [88] T. Mizoguchi and M. Udagawa, *Phys. Rev. B* **99**, 235118 (2019).
- [89] Z. Ma, S. Li, Y.-W. Zheng, M.-M. Xiao, H. Jiang, J.-H. Gao, and X. Xie, *Science Bulletin* **66**, 18 (2021).
- [90] R. Makov, F. Guinea, and A. Stern, *Phys. Rev. B* **110**, 195112 (2024).
- [91] D. Vanderbilt, *Berry phases in electronic structure theory: electric polarization, orbital magnetization and topological insulators* (Cambridge University Press, 2018).